Original Article

Peptidyl-prolyl isomerase F as a prognostic biomarker associated with immune infiltrates and mitophagy in lung adenocarcinoma

Zitong Feng[1,2]^, Lin Yuan[3]^, Luyuan Ma[1,2], Wenhao Yu[1,2], Fayez Kheir[4], Lukas Käsmann[5,6,7], Wolfgang M. Brueckl[8], Kai Jin[1,2], Dingxin Wang[1,2], Yi Shen[1,2], Rongyang Li[1,2], Hui Tian[1]

[1]Department of Thoracic Surgery, Qilu Hospital of Shandong University, Jinan, China; [2]Laboratory of Basic Medical Sciences, Qilu Hospital of Shandong University, Jinan, China; [3]Department of Clinical Laboratory Medicine, The First Affiliated Hospital of Shandong First Medical University & Shandong Provincial Qianfoshan Hospital, Shandong Medicine and Health Key Laboratory of Laboratory Medicine, Jinan, China; [4]Division of Pulmonary and Critical Care Medicine, Massachusetts General Hospital, Harvard Medical School, Boston, MA, USA; [5]Department of Radiation Oncology, University Hospital, LMU Munich, Munich, Germany; [6]Comprehensive Pneumology Center Munich (CPC-M), Member of the German Center for Lung Research (DZL), Munich, Germany; [7]German Cancer Consortium (DKTK), Partner Site Munich, Munich, Germany; [8]Department of Respiratory Medicine, Allergology and Sleep Medicine, Paracelsus Medical University, General Hospital Nuernberg, Nuremberg, Germany

Contributions: (I) Conception and design: Z Feng, H Tian; (II) Administrative support: L Yuan, H Tian; (III) Provision of study materials or patients: L Ma, W Yu, K Jin; (IV) Collection and assembly of data: L Yuan, D Wang, Y Shen; (V) Data analysis and interpretation: W Yu, R Li; (VI) Manuscript writing: All authors; (VII) Final approval of manuscript: All authors.

Correspondence to: Hui Tian, MD. Department of Thoracic Surgery, Qilu Hospital of Shandong University, No. 107 Wen Hua Xi Road, Jinan 250012, China. Email: tianhuiql@email.sdu.edu.cn.

Background: Lung adenocarcinoma (LUAD) is among the most prevalent malignancies worldwide, with unfavorable treatment outcomes. Peptidyl-prolyl isomerase F (*PPIF*) is known to influence the malignancy traits of tumor progression by modulating the bioenergetics and mitochondrial permeability in cancer cells; however, its role in LUAD remains unclear. Our study seeks to investigate the clinical significance, tumor proliferation, and immune regulatory functions of *PPIF* in LUAD.

Methods: The expression of *PPIF* in LUAD tissues and cells was assessed using bioinformatics analysis, immunohistochemistry (IHC), and Western blotting. Survival curve analysis was conducted to examine the prognostic association between *PPIF* expression and LUAD. The immunomodulatory role of *PPIF* in LUAD was assessed through the analysis of *PPIF* expression and immune cell infiltration. A series of gain- and loss-of-function experiments were conducted on *PPIF* to investigate its biological functions in LUAD both *in vitro* and *in vivo*. The mechanisms underlying *PPIF*'s effects on LUAD were delineated through functional enrichment analysis and Western blotting assays.

Results: *PPIF* exhibited overexpression in LUAD tissues compared to normal controls. Survival curve analysis revealed that patients with LUAD exhibiting higher *PPIF* expression demonstrated decreased overall survival and a shorter progression-free interval. *PPIF* was implicated in modulating immune cell infiltration, particularly in regulating the T helper 1–T helper 2 cell balance. Functionally, *PPIF* was discovered to promote tumor cell proliferation and advance cell-cycle progression. Furthermore, *PPIF* could impede mitophagy by targeting the FOXO3a/PINK1–Parkin signaling pathway.

Conclusions: The findings of this study indicate that the prognosis-related gene *PPIF* may have a significant role in the regulation of LUAD cell proliferation, tumor-associated immune cell infiltration, and mitophagy, and thus *PPIF* may be a promising therapeutic target of LUAD.

Keywords: Peptidyl-prolyl isomerase F (*PPIF*); lung adenocarcinoma (LUAD); prognosis; immune; mitophagy

^ ORCID: Zitong Feng, 0000-0003-1797-6782; Lin Yuan, 0009-0004-9321-6755.

Submitted Apr 17, 2024. Accepted for publication Jun 05, 2024. Published online Jun 20, 2024.
doi: 10.21037/tlcr-24-344
View this article at: https://dx.doi.org/10.21037/tlcr-24-344

Introduction

Lung adenocarcinoma (LUAD), a predominant subtype of non-small cell lung cancer (NSCLC), presents substantial challenges in prognosis and treatment despite recent advances in targeted and immune therapies (1-3). Although tyrosine kinase inhibitors (TKIs) and immune checkpoint inhibitors (ICIs) have improved outcomes for select patient populations, the heterogeneity of LUAD and the emergence of resistance underscore the need for more precise biomarkers to guide therapy. To date, established prognostic markers such as EGFR mutation status and programmed cell death ligand 1 (PD-L1) expression have been instrumental in personalizing treatment, yet they do not fully capture the complexity of disease progression or therapeutic response. As a result, there is an imperative need to identify additional prognostic markers that could refine patient stratification and target discovery.

Cyclophilin D (CypD), encoded by the peptidyl-prolyl isomerase F (*PPIF*) gene, is primarily recognized for regulating the mitochondrial permeability transition pore (mPTP) opening threshold, thereby contributing to apoptotic signaling and cell necrosis (4,5). *PPIF*, induced by exogenous stimuli, suppresses cell apoptosis via interaction with B-cell lymphoma 2 (BCL-2) (6). Previous studies have reported that a wide array of cancer cells, such as those originating in the breast, ovary, and uterus, exhibit overexpression of CypD (7). For instance, overexpression of *PPIF* was found to be related to poor survival in endometrial cancer (8). Moreover, in osteosarcoma, cinnamtannin B-1-induced downregulation of *PPIF* correlates with tumor growth inhibition, thus highlighting the significance of *PPIF* in cellular proliferation (9). Currently, the role of *PPIF* in LUAD, specifically its influence on tumor immune cell infiltration, cell proliferation, prognosis, and underlying molecular mechanisms, remains to be elucidated.

Drawing on data from publicly accessible databases, our study found that *PPIF* was markedly overexpressed in LUAD and that high *PPIF* expression exhibited prognostic value in patients with LUAD. Both *in vitro* and *in vivo* experiments showed that *PPIF* facilitates the proliferation of LUAD cells. Our results also indicated that *PPIF* could modulate immune cell infiltration and mitophagy. These findings may offer novel insights into enhancing the therapeutic efficacy of LUAD treatments by targeting *PPIF*, potentially benefiting their future clinical application. We present this article in accordance with the ARRIVE and MDAR reporting checklists (available at https://tlcr.amegroups.com/article/view/10.21037/tlcr-24-344/rc).

Highlight box

Key findings

- Peptidyl-prolyl isomerase F (*PPIF*) was overexpressed in lung adenocarcinoma (LUAD) relative to normal tissues, which markedly enhanced the proliferative capacity of LUAD cells. These findings indicate that *PPIF* could be a potential therapeutic target for LUAD.

What is known and what is new?

- Cyclophilin D (CypD), encoded by the *PPIF* gene, is predominantly acknowledged for its role in modulating the mitochondrial permeability transition pore (mPTP) opening threshold.
- *PPIF* may play an important role in the recruitment of immune cells in LUAD, potentially influencing the tumor microenvironment by modulating the T helper 1–T helper 2 (Th1/Th2) cell balance. *PPIF* functions as a regulator of mitophagy and is critical to tumor initiation and progression.

What is the implication, and what should change now?

- *PPIF* is involved in the regulation of the Th1/Th2 cell balance within the tumor microenvironment of lung tumors. Further studies are imperative to elucidate the precise mechanisms of action and the potential therapeutic significance of *PPIF* in patients with LUAD.

Methods

Public databases and online websites

The RNA sequencing (RNA-Seq) data from The Cancer Genome Atlas (TCGA) (10) (https://portal.gdc.cancer.gov/) and the Genotype-Tissue Expression (GTEx) (https://www.gtexportal.org/home/-index.html) database, harmonized in transcripts per million (TPM), was procured from the UCSC Xena (https://xenabrowser.net/datapages/) platform. We examined the expression levels of the *PPIF* gene in a range of tumors and normal tissues using these integrated

datasets. We sourced the RNA expression profiles and clinical data of patients with LUAD from TCGA database. Subsequently, the RNA-seq data were transformed into TPM format for standardized quantification. Our analysis involved a total of 539 LUAD samples and 59 healthy controls registered in TCGA database. The gene expression profiling data sets (GSE7670, GSE10072, GSE19804, GSE31547, GSE40791, GSE116959, GSE27262) were obtained from the Gene Expression Omnibus (GEO) database (https://www.ncbi.nlm.nih.gov/gds). The protein–protein interaction (PPI) network we employed for enrichment analysis was downloaded from the Biological General Repository for Interaction Datasets (BioGRID) website (11) (https://thebiogrid.org/). The top 200 *PPIF*-correlated genes in LUAD were obtained through the "similar gene detection" module on the Gene Expression Profiling Interactive Analysis 2 (GEPIA2) website (http://gepia2.cancer-pku.cn/). To assess the prognostic potential of *PPIF* in various immune cell subsets within LUAD cohorts, we employed the Kaplan-Meier Plotter tool (12) (https://kmplot.com).

Data processing

The R programming language (version 4.0.4) was predominantly applied for the data analysis conducted throughout this study. Data visualization was performed using the "ggplot2" package (version 3.3.6), proportional hazard assumption testing and fitting survival regression were carried out with the "survival" package (version 3.3.1), and functional enrichment analyses, including Gene Ontology (GO) (13) and Kyoto Encyclopedia of Genes and Genomes (KEGG) (14) pathways, were carried out using the "clusterProfiler" package (version 4.4.4). Based on the single-sample gene set enrichment analysis (ssGSEA) (15) algorithm provided in the "GSVA" package (version 1.46.0) (16), we used the markers for 24 immune cells (17) to calculate the immune infiltration status of corresponding TCGA data.

Patient specimens and tissue microarray

Ten pairs of fresh LUAD tissue samples and adjacent normal tissue samples were obtained from Department of Thoracic Surgery, Qilu Hospital of Shandong University between June 2020 and December 2020 for immunoblotting analysis. All postoperative LUAD tissues were confirmed by pathological analysis and stored in liquid nitrogen for subsequent protein extraction. This study was approved by the Medical Ethics Committee of Qilu Hospital of Shandong University (No. KYLL-202008-023-1) and was conducted in accordance with the Helsinki Declaration (as revised in 2013). Informed consent was obtained from each participant or their authorized proxies. A tissue microarray (HLugA180Su11) comprising 89 paired LUAD tissues and adjacent normal tissues was purchased from Shanghai Outdo Biotech. This microarray includes complete clinical prognosis information for each sample. Ethical clearance for using this resource was obtained from the Ethics Committee of Shanghai Outdo Biotech Company (SHYJS-CP-2206001).

Immunohistochemistry (IHC) and hematoxylin and eosin (HE) staining

Tissues obtained from patients with LUAD and tumors from nude mice were fixed in 4% paraformaldehyde at room temperature for 1 h and then cut into 4-μm sections. For HE staining, each section was deparaffinized, rehydrated, and stained with HE. For IHC procedures, each tissue section underwent dewaxing and rehydration and then overnight incubation with primary antibodies at 4 ℃ and subsequent incubation with a secondary antibody at room temperature for 1 hour. Representative photomicrographs were captured using an inverted microscope. The IHC scoring standard was determined using the histochemistry score, which was calculated as follows: histochemistry score = staining intensity (0, none; 1, weak; 2, moderate; 3, strong) × percentage of positive cells (0–100%). The following antibodies were used in this study: anti-*PPIF* (1:100; cat no. 45-5900; RRID: AB_2533820; Invitrogen, Thermo Fisher Scientific, Carlsbad, CA, USA) and anti-Ki-67 (1:500, cat no. ET1609-34; RRID: AB_3069844; HUABIO, Hangzhou, China).

Cell culture and treatment

Human LUAD cell lines H1975 (cat no. FH0086), A549 (cat no. FH0045), PC9 (cat no. FH1002), and H1299 (cat no. FH0908) were purchased from the Shanghai Fuheng Biotechnology Co., Ltd, and cultured in Dulbecco's Modified Eagle Medium (DMEM)/F-12 with 10% fetal bovine serum (FBS; Gibco, Grand Island, NY, USA at 37 ℃ in a 5% CO_2 atmosphere. Cells were transfected with small interfering RNAs (siRNAs) (GenePharma, Shanghai, China) or overexpression plasmids (Research Cloud Biology) using

jetPRIME transfection reagent (Polyplus, Illkirch, France) according to the manufacturer's instructions. The siRNA template sequences were applied as follows: si*PPIF*_1, sense CUGACGAGAACUUUACACUTT; si*PPIF*_1, antisense AGUGUAAAGUUCUCGUCAGTT; si*PPIF*_2, sense CAAGCAUGUUGUGUUCGGUTT; and si*PPIF*_2, antisense ACCGAACACAACAUGCUUGTT. The si*PPIF*_1 sequence was used for lentivirus packaging (Jikai Corporation, Shanghai, China). Lentiviral transduction was performed according to the manufacturer's instructions, and stably transduced cells were selected with 4 μg/mL puromycin for 3 days.

Real-time quantitative polymerase chain reaction

The total cellular RNA was extracted using the RNAfast200 Kit (Fastagen Biotech, Shanghai, China), which was followed by reverse transcription performed with the AG11706 kit (Accurate Biology, Hunan, China). Subsequent real-time quantitative polymerase chain reaction (RT-qPCR) was conducted using the Bio-Rad IQ5 RT-PCR detection system and the SYBR Green Premix Pro Taq HS qPCR Kit (AG11701; Accurate Biology). The following primers were procured from Biosune Company: *PPIF* (forward 5'-AAGTOCATCTACGGAAGOCG-3', reverse 5'-TGCTTGCCATCCAACCAGTC-3') and *GAPDH* (forward 5'-GCACCGTCAAGGCTGAGAAC-3', reverse 5'-TGGTGAAGACGCCAGTGGA-3'). The expression levels of the target genes were assessed using the $2^{-\Delta\Delta Ct}$ method. The experiment was conducted in triplicate.

Western blotting assay

Proteins from the cells and LUAD tissues were extracted through lysis in RIPA buffer (Beyotime, Shanghai, China). Protein lysates were separated using 10% or 12% sodium dodecyl sulfate polyacrylamide gel electrophoresis (SDS-PAGE) gels and then electrically transported to polyvinylidene difluoride (PVDF) membranes. The membranes were incubated with 5% nonfat milk for 1 hour to block nonspecific sites before the application of primary antibodies. Following incubation with the corresponding secondary antibodies, the membranes were visualized using an enhanced chemiluminescence (ECL) detection system. This study used the following antibodies: anti-β-tubulin (1:5,000; cat. no. EM0103, RRID: AB_2819165; HUABIO), anti-*PPIF* (1:1,000; cat. no. 45-5900l RRID: AB_2533820; Invitrogen), anti-cyclin D1 (1:5,000, cat. no. ET1601-31; RRID: AB_3069614; HUABIO), anti-CDK1 (1:2,000; cat. no. ET1605-54; RRID: AB_3069718; HUABIO), anti-CDK4 (1:1,000; cat. no. ET1612-23; RRID: AB_3070096; HUABIO), anti-cyclin E1 (1:1,000; cat. no. ET1612-16; RRID: AB_3070088; HUABIO), anti-FOXO3a (1:1,000; cat. no. ET1604-11; RRID: AB_3069686; HUABIO), anti-PINK1 (1:1,000; cat. no. ab216144; RRID: AB_292772; Abcam, UK), anti-P62 (1:1,000; cat. no. HA721171; RRID: AB_3072293; HUABIO), anti-Parkin (1:1,000; cat. no. ET1702-60; RRID: AB_3070322; HUABIO), anti-Atg5 (1:1,000; cat. no. ET1611-38; RRID: AB_3070016; HUABIO), and anti-LC3B (1:1,000; cat. no. ET1701-65, RRID: AB_3070229; HUABIO).

Cell counting kit-8 (CCK-8), colony formation, and 5-ethynyl-2'-deoxyuridine assay

Cell viability was assessed using the CCK-8 assay (Apexbio, Houston, TX, USA) according to the manufacturer's protocol, with absorbance measurements taken at 450 nm using a microplate reader. In each well of six-well plates, 800 cells were seeded and cultivated for 14 days to facilitate colony development. After incubation, formed colonies were fixed with 4% paraformaldehyde and subsequently stained with 0.5% crystal violet solution. LUAD cells (1×10^4) were cultured overnight in 96-well plates. DNA synthesis was examined using the EdU Cell Proliferation Kit (Beyotime), and the proliferation rate was determined under a fluorescence microscope. The proliferation rate was quantified by analyzing fluorescence microscopy images. All assays were conducted in triplicate to ensure experimental reliability.

In vivo experiments

A protocol was prepared before the study without registration. All animal experiments were approved by the Ethics Committee of Animal Experiment of Qilu Hospital of Shandong University (No. DWLL-2023-056), and were conducted in accordance with institutional guidelines for the care and use of animals. Four-week-old female BALB/cNj-Foxn1^{nu}/Gpt nude mice (strain no. D000521) were supplied by Gempharmatech Co., Ltd. For the establishment of the xenograft tumor model, 10 nude mice were randomly assigned to 2 groups. Subsequently, PC9 cells transduced with stable expressions of sh-*PPIF* or sh-NC (negative control) were injected subcutaneously into the right axillary region of each mouse. Housing and husbandry

practices adhered strictly to the standards outlined in the *Guide for the Care and Use of Laboratory Animals* [2011]. Tumor size was measured at 6-day intervals, and tumor volume was estimated using the formula: volume = (length × width^2)/2. After 24 days, the mice were euthanized through decapitation while under anesthesia, which was induced by an intraperitoneal injection of phenobarbital (100 mg/kg). Subsequently, the tumors were harvested and weighed.

Flow cytometry analysis and electron microscopy

Cell-cycle assays were conducted using the Cell Cycle Assay Kit (Lianke Pharmaceutical Co., Ltd., Hangzhou, China) following the manufacturer's guidelines. Flow cytometry analysis was performed using a CytoFLEX instrument (Beckman Coulter). After digestion and collection, the cells were fixed with 3% glutaraldehyde. Finally, cell samples were refixed with 1% osmium tetroxide, gradually dehydrated in a series of acetone solutions, and embedded in Ep812 resin. Following staining, the samples were sectioned using a diamond knife. Image acquisition was carried out using the JEM-1400FLASH transmission electron microscope (JEOL).

Statistical analysis

Statistical analyses were conducted using R software (version 4.0.4) and GraphPad Prism version 9.0 (GraphPad Software). X-tile software (version 1.0.4; http://kinzler.com/me/xtitle) was employed to determine an appropriate cutoff value. For survival data, the log-rank test and Kaplan-Meier survival analysis were employed. Categorical comparisons were conducted using Pearson chi-squared test, while continuous variables were assessed with a two-tailed Student *t*-test or Wilcoxon rank sum test. Bonferroni correction method was applied when conducting multiple statistical comparisons. Fisher exact test was applied for small-sample categorical comparisons, and Pearson correlation analysis was employed to evaluate relationships between variables. One-way analysis of variance (ANOVA) was applied to evaluate the differences between more than two groups. All data are presented as mean ± standard deviation (SD). Each experiment was independently conducted with three biological replicates. $P<0.05$ or $P<\alpha/n$ (α is the original significance level and n is the number of comparisons performed) was deemed indicative of a statistically significant difference.

Results

Upregulation of PPIF expression in LUAD tissues

According to TCGA database and GTEx database, we found *PPIF* to be highly expressed in many different types of cancers, including LUAD, lung squamous cell carcinoma, breast invasive carcinoma, stomach adenocarcinoma, colon adenocarcinoma, and brain lower grade glioma, among others (*Figure 1A*). To specifically investigate LUAD, we compared the messenger RNA (mRNA) level of *PPIF* in LUAD tissues and normal lung tissues in various datasets. In both TCGA and several GEO datasets (GSE7670, GSE10072, GSE19804, GSE31547, GSE40791, GSE116959, GSE27262), the mRNA levels of *PPIF* were significantly upregulated in LUAD tissues (*Figure 1B*). Subsequently, we analyzed a tissue microarray comprising 89 paired LUAD tissues and adjacent normal tissues to evaluate the extent of PPIF protein expression (*Figure 1C*). According to the IHC score, PPIF protein expression was significantly elevated in LUAD tissues compared to normal lung tissues (*Figure 1B*). Additionally, Western blotting assays confirmed the elevated PPIF protein expression levels in 10 LUAD tissues relative to their paired normal tissues (*Figure 1D*). Collectively, these data indicate that *PPIF* is highly expressed in LUAD and underscores its potential significance in LUAD.

Identification of PPIF as an independent prognostic indicator in LUAD

TCGA database was used to explore the prognostic significance of *PPIF* mRNA expression levels in LUAD patients. *Table 1* presents the correlations between *PPIF* mRNA expression and clinicopathological factors in 539 patients with LUAD. Results from the chi-squared test indicated significant associations between *PPIF* mRNA expression and gender (P=0.004), pathologic T stage (P=0.002), pathologic N stage (P=0.02), and pathologic stage (P=0.001). However, no significant correlations were found with age, smoking status, tumor location, or pathologic M stage. According to the Kaplan-Meier survival analysis, patients with higher expression levels of *PPIF* exhibited a poorer overall survival (*Figure 2A*) and progression-free interval (*Figure 2B*). *PPIF* mRNA expression was found to be a significant negative prognostic factor for overall survival in univariate [hazard ratio (HR) =1.506, 95% CI: 1.126–2.012; P=0.006] and multivariate Cox regression analyses (HR =1.462, 95% CI: 1.032–2.070; P=0.03) (*Table 2*).

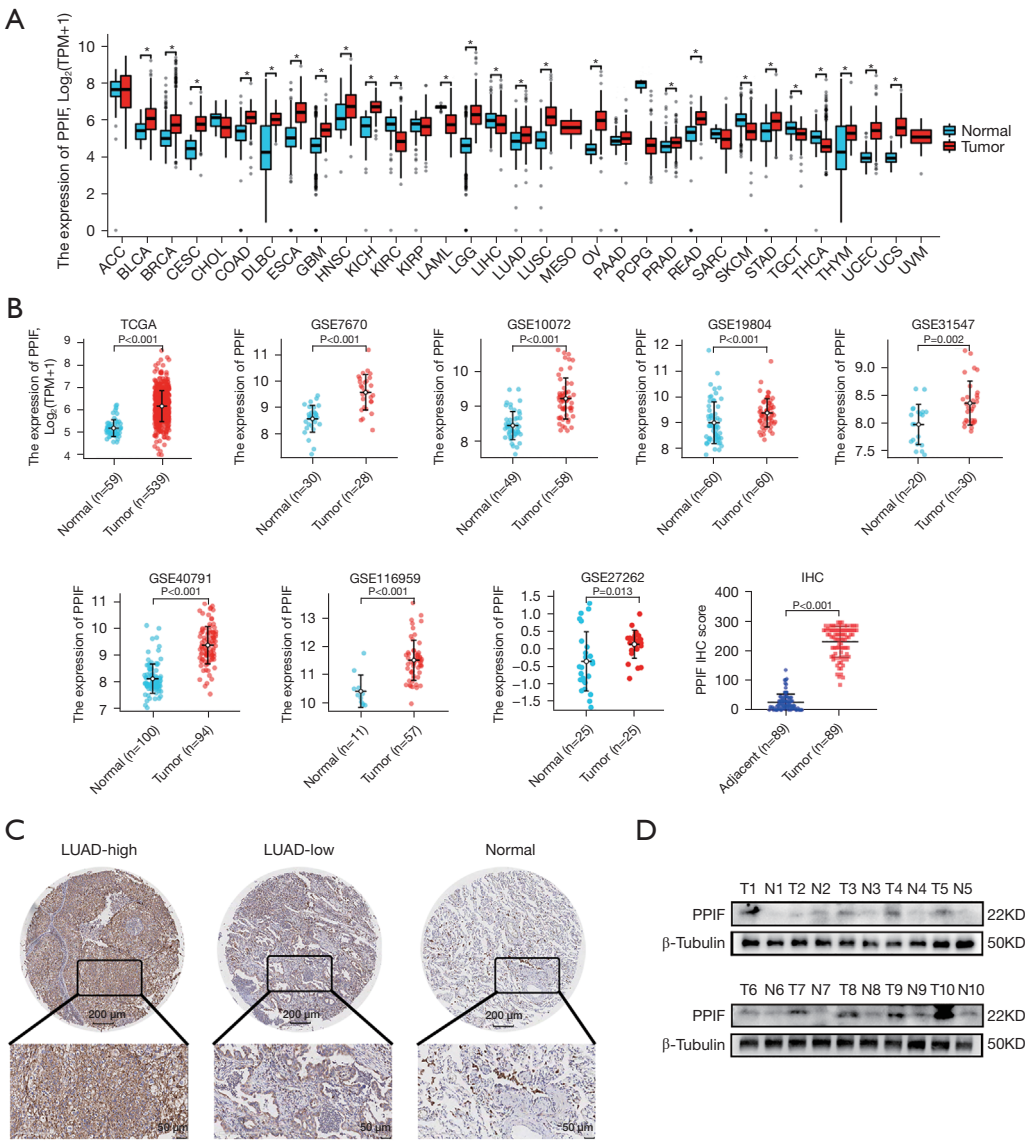

Figure 1 Analysis of *PPIF* expression status. (A) *PPIF* mRNA expression in different types of tumor tissues and normal tissues based on the GTEx and TCGA databases. (B) The expression of *PPIF* was upregulated in LUAD tissues according to TCGA, several GEO databases, and the tissue microarray. (C) Representative IHC images of *PPIF* expression in LUAD tissues and normal tissues. (D) Representative Western blotting images on the protein levels of *PPIF* in 10 pairs of LUAD tissues and normal tissues. *, P<α', α'=0.05/30. TPM, transcripts per million; *PPIF*, peptidyl-prolyl isomerase F; GTEx, Genotype-Tissue Expression; TCGA, The Cancer Genome Atlas; ACC, adrenocortical carcinoma; BLCA, bladder urothelial carcinoma; BRCA, breast invasive carcinoma; CESC, cervical squamous cell carcinoma and endocervical adenocarcinoma; CHOL, cholangio carcinoma; COAD, colon adenocarcinoma; DLBC, lymphoid neoplasm diffuse Large B-cell Lymphoma; ESCA, esophageal carcinoma; GBM, glioblastoma multiforme; HNSC, head and neck squamous cell carcinoma; KICH, kidney chromophobe; KIRC, kidney renal clear cell carcinoma; KIRP, kidney renal papillary cell carcinoma; LAML, acute myeloid leukemia; LGG, brain lower grade glioma; LIHC, liver hepatocellular carcinoma; LUSC, lung squamous cell carcinoma; LUAD, lung adenocarcinoma; MESO, mesothelioma; OV, ovarian serous cystadenocarcinoma; PAAD, pancreatic adenocarcinoma; PCPG, pheochromocytoma and paraganglioma; PRAD, prostate adenocarcinoma; READ, rectum adenocarcinoma; SARC, sarcoma; SKCM, skin cutaneous melanoma; STAD, stomach adenocarcinoma; TGCT, testicular germ cell tumors; THCA, thyroid carcinoma; THYM, thymoma; UCEC, uterine corpus endometrial carcinoma; UCS, uterine carcinosarcoma; UVM, uveal melanoma; GEO, Gene Expression Omnibus; IHC, immunohistochemical.

Table 1 Clinicopathological characteristics of patients with LUAD exhibiting differential *PPIF* expression

Characteristics	Low expression of *PPIF* (n=269)	High expression of *PPIF* (n=270)	P value
Age, n (%)			0.86
≤65 years	131 (25.2)	126 (24.2)	
>65 years	132 (25.4)	131 (25.2)	
Gender, n (%)			0.004
Female	161 (29.9)	128 (23.7)	
Male	108 (20)	142 (26.3)	
Smoker, n (%)			0.16
No	44 (8.4)	33 (6.3)	
Yes	217 (41.3)	231 (44)	
Tumor location, n (%)			0.95
Central lung	24 (12.6)	39 (20.5)	
Peripheral lung	49 (25.8)	78 (41.1)	
Pathologic T stage, n (%)			0.002
T1	105 (19.6)	71 (13.2)	
T2	139 (25.9)	153 (28.5)	
T3	18 (3.4)	31 (5.8)	
T4	5 (0.9)	14 (2.6)	
Pathologic N stage, n (%)			0.02
N0	188 (35.9)	162 (31)	
N1	39 (7.5)	58 (11.1)	
N2	28 (5.4)	46 (8.8)	
N3	1 (0.2)	1 (0.2)	
Pathologic M stage, n (%)			0.27
M0	173 (44.4)	192 (49.2)	
M1	9 (2.3)	16 (4.1)	
Pathologic stage, n (%)			0.001
Stage I	170 (32)	126 (23.7)	
Stage II	54 (10.2)	71 (13.4)	
Stage III	31 (5.8)	53 (10)	
Stage IV	10 (1.9)	16 (3)	

LUAD, lung adenocarcinoma; *PPIF*, peptidyl-prolyl isomerase F.

Both univariate and multivariate Cox regression analyses also identified pathologic T stage, pathologic N stage, and *PPIF* expression as significant prognostic factors for overall survival. Additionally, Kaplan-Meier curve analysis of a tissue microarray cohort demonstrated a significant negative association between PPIF protein expression and overall survival (*Figure 2C*). In summary, these findings suggest a potential cancer-promoting role for *PPIF* in LUAD.

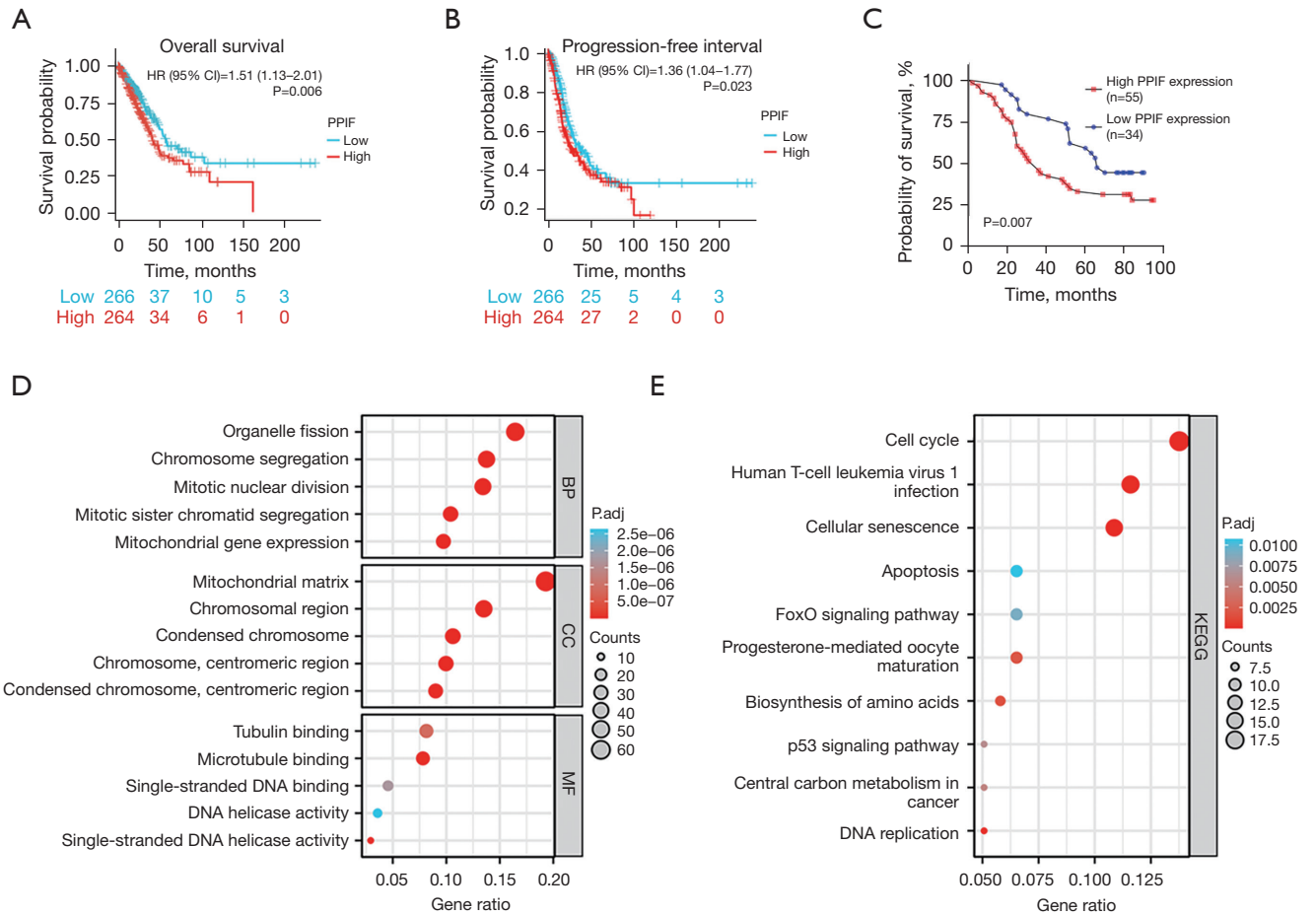

Figure 2 *PPIF* was associated with patients' prognosis and performs a variety of biological functions in LUAD. Kaplan-Meier curves for overall survival (A) and progression-free interval (B) in TCGA patients. (C) Kaplan-Meier analysis comparing overall survival between the high- and low-*PPIF* expression groups in tissue microarray patients. GO enrichment (D) and KEGG (E) enrichment analysis by the *PPIF*-correlated gene. HR, hazard ratio; BP, biological process; CC, cellular component; MF, molecular function; KEGG, Kyoto Encyclopedia of Genes and Genomes; *PPIF*, peptidyl-prolyl isomerase F; LUAD, lung adenocarcinoma; TCGA, The Cancer Genome Atlas; GO, Gene Ontology.

Functional inference of PPIF in LUAD

To investigate the molecular mechanisms underlying *PPIF*-induced carcinogenesis in LUAD, we performed PPI network analysis using the BioGRID database. Figure S1A depicts the interaction network of 142 *PPIF*-binding proteins. Furthermore, we employed the "similar gene detection" module of GEPIA2 to analyze the analogous genes of *PPIF* in LUAD, with the resulting heatmap presenting the hierarchical clustering analysis of the top 20 similar genes (Figure S1B). We conducted GO and KEGG enrichment analysis by integrating a total of 342 genes, consisting of the 142 interaction genes and the 200 coexpressed genes. In the biological processes (BP) category, the gene clusters were involved in processes such as mitotic nuclear division, chromosome segregation, and mitotic sister chromatid segregation. In the cellular components (CC) category, the total genes were enriched in mitochondrial matrix, chromosomal region, and condensed chromosome. In terms of molecular function (MF), the genes were involved in microtubule binding, single-stranded DNA binding, and single-stranded DNA helicase activity (*Figure 2D*). *Figure 2E* displays the results of the KEGG pathway analysis, indicating enrichment in pathways such as the cell cycle, p53 signaling, and FoxO signaling. The enrichment analysis supported the potential involvement of

Table 2 Cox regression analysis for clinical outcomes in patients with LUAD

Characteristic	Number of patients	Univariate analysis		Multivariate analysis	
		Hazard ratio (95% CI)	P value	Hazard ratio (95% CI)	P value
Age (years)	520	1.216 (0.910–1.625)	0.19		
≤65	257				
>65	263				
Gender	530	1.087 (0.816–1.448)	0.57		
Female	283				
Male	247				
Smoker	516	0.942 (0.625–1.420)	0.78		
No	74				
Yes	442				
Location	183	0.949 (0.593–1.520)	0.83		
Central lung	63				
Peripheral lung	120				
Pathologic T stage	527	2.352 (1.614–3.426)	<0.001	1.712 (1.072–2.732)	0.02
T1 & T2	461				
T3 & T4	66				
Pathologic N stage	514	2.547 (1.904–3.407)	<0.001	1.900 (1.284–2.812)	0.001
N0	345				
N1 & N2 & N3	169				
Pathologic M stage	381	2.176 (1.272–3.722)	0.005	1.187 (0.624–2.258)	0.60
M0	356				
M1	25				
Pathologic stage	522	2.710 (1.994–3.685)	<0.001	1.565 (0.958–2.555)	0.07
Stage I & stage II	415				
Stage III & stage IV	107				
PPIF	530	1.506 (1.126–2.012)	0.006	1.462 (1.032–2.070)	0.03
Low	266				
High	264				

LUAD, lung adenocarcinoma; *PPIF*, peptidyl-prolyl isomerase F; CI, confidence interval.

PPIF in mitosis and cell proliferation.

Association between PPIF expression and infiltrating immune cells

To investigate the association between *PPIF* and the tumor microenvironment, we implemented the ssGSEA algorithm to characterize the relationship between *PPIF* gene expression and the infiltration levels of 24 immune cell types. As shown in *Figure 3A*, T helper 2 (Th2) cells, γδ T cells (Tgd), and CD56dim natural killer (NK) cells were positively correlated with *PPIF* expression. However, T follicular helper (TFH) cells, mast cells, and B cells exhibited a significant negative association with *PPIF*.

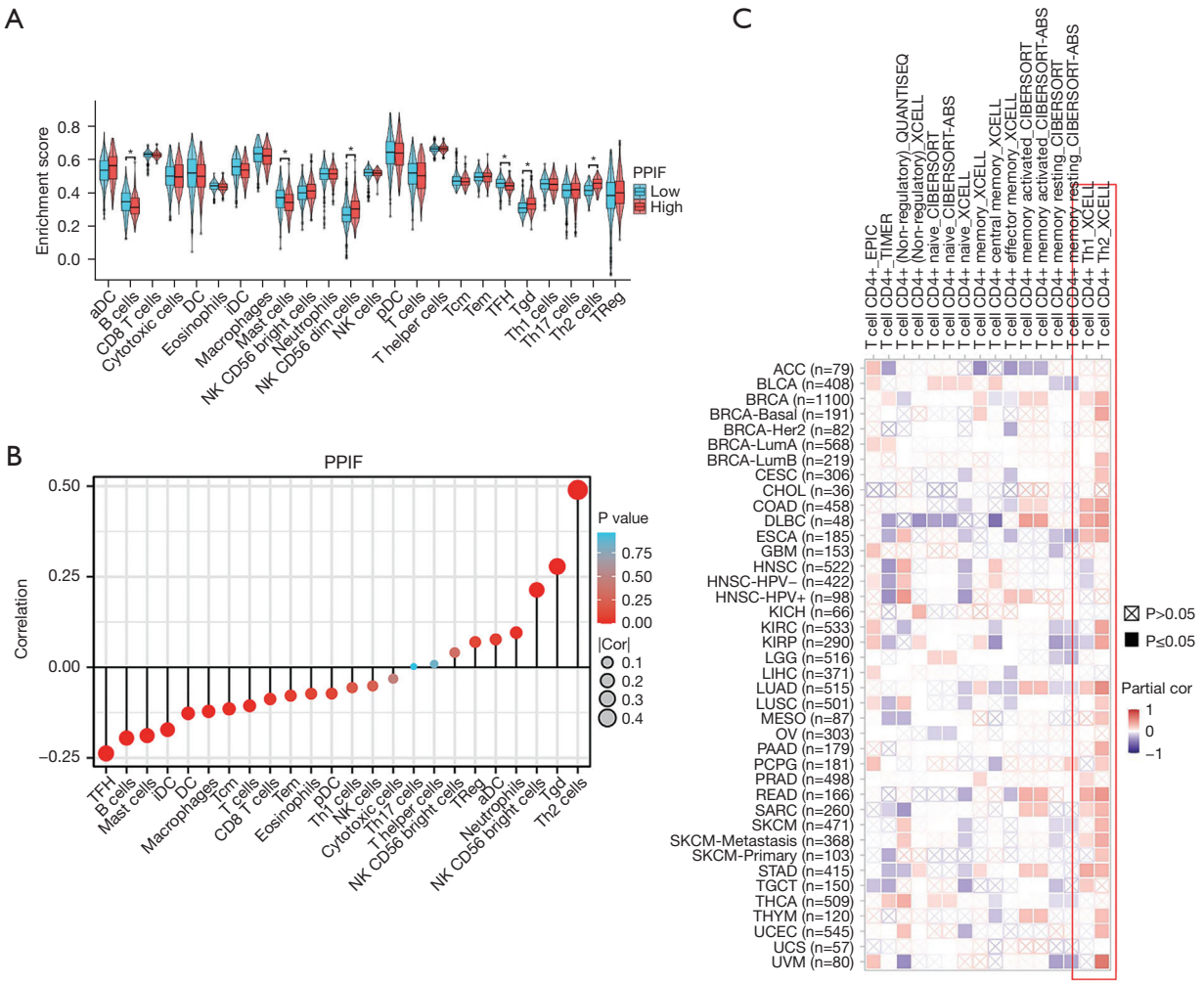

Figure 3 Immune infiltration analysis of *PPIF*. (A) Different levels of 24 subtypes of immune cells in the high and low *PPIF* expression groups in LUAD tissue samples. (B) The correlation between *PPIF* expression level and 24 immune cell types in LUAD tissues. (C) The potential relationship between T-cell infiltration and *PPIF* gene expression in various cancer types. *, P<α', α'=0.05/24. aDC, activated dendritic cells; DC, dendritic cells; iDC, immature dendritic cells; NK, natural killer cells; pDC, plasmacytoid dendritic cells; Tcm, T central memory; Tem, T effector memory; TFH, T follicular helper; Tgd, γδ T cells; Th1, T helper 1; Th17, T helper 17; Th2, T helper 2; ACC, adrenocortical carcinoma; BLCA, bladder urothelial carcinoma; BRCA, breast invasive carcinoma; CESC, cervical squamous cell carcinoma and endocervical adenocarcinoma; CHOL, cholangio carcinoma; COAD, colon adenocarcinoma; DLBC, lymphoid neoplasm diffuse large B-cell lymphoma; ESCA, esophageal carcinoma; GBM, glioblastoma multiforme; HNSC, head and neck squamous cell carcinoma; KICH, kidney chromophobe; KIRC, kidney renal clear cell carcinoma; KIRP, kidney renal papillary cell carcinoma; LGG, brain lower grade glioma; LIHC, liver hepatocellular carcinoma; LUSC, lung squamous cell carcinoma; LUAD, lung adenocarcinoma; MESO, mesothelioma; OV, ovarian serous cystadenocarcinoma; PAAD, pancreatic adenocarcinoma; PCPG, pheochromocytoma and paraganglioma; PRAD, prostate adenocarcinoma; READ, rectum adenocarcinoma; SARC, sarcoma; SKCM, skin cutaneous melanoma; STAD, stomach adenocarcinoma; TGCT, testicular germ cell tumors; THCA, thyroid carcinoma; THYM, thymoma; UCEC, uterine corpus endometrial carcinoma; UCS, uterine carcinosarcoma; UVM, uveal melanoma; *PPIF*, peptidyl-prolyl isomerase F.

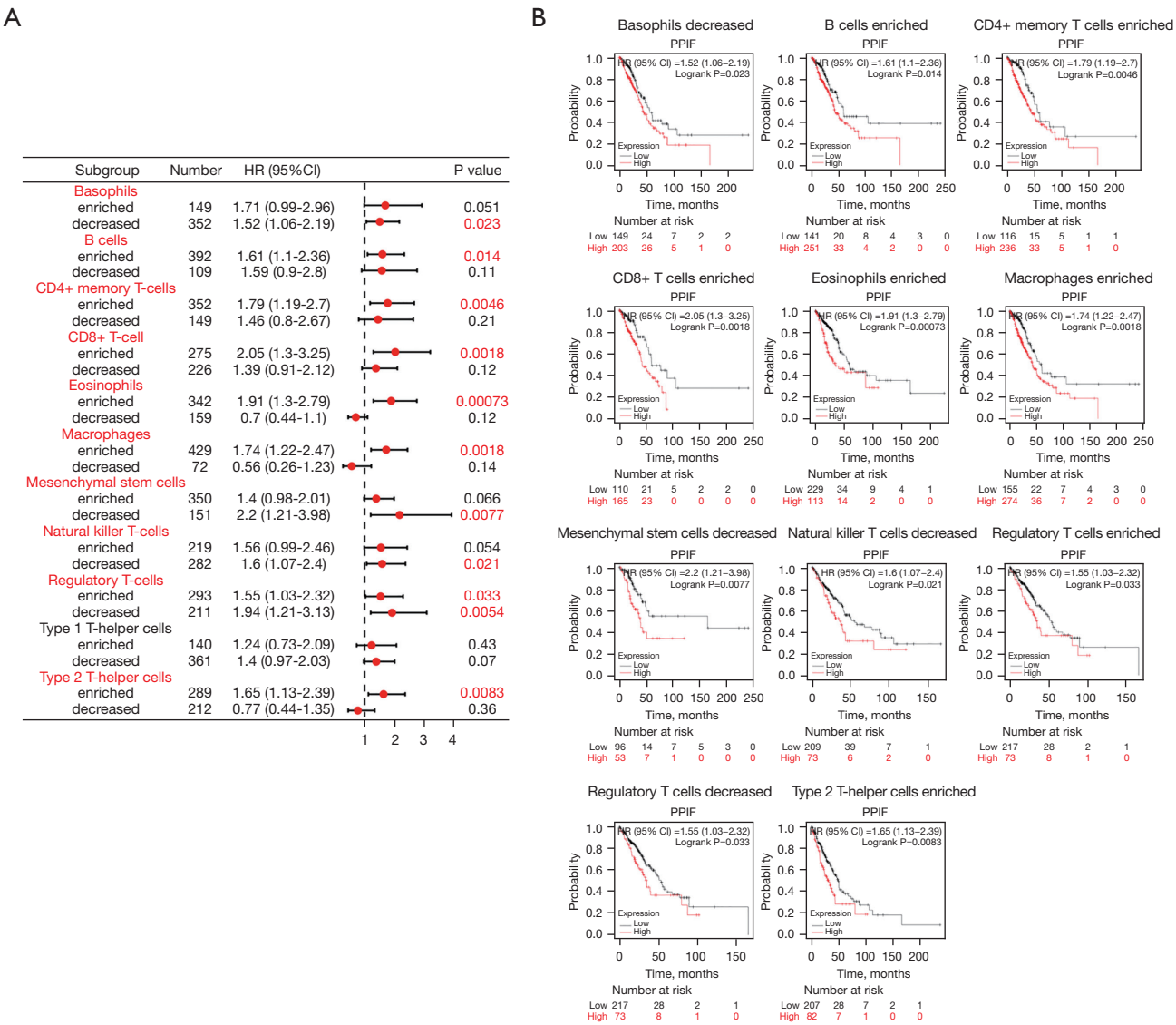

Figure 4 Kaplan-Meier survival analysis of patients with LUAD exhibiting high and low expression of *PPIF* under different immune cell subsets. (A) Forest plot of survival analysis of HR and P values under different immune cell subsets. Subgroup names and P values with statistical significance are displayed in red. (B) Kaplan-Meier survival curves under 11 immune cell subsets. HR, hazard ratio; CI, confidence interval; LUAD, lung adenocarcinoma; *PPIF*, peptidyl-prolyl isomerase F.

Figure 3B further illustrates the relationship between *PPIF* expression and immune cell infiltration, with the expression of *PPIF* being the most correlated with Th2 cells among the 24 immune cell types. These results suggest that *PPIF* may influence the tumor microenvironment by shifting the Th1/Th2 cell balance in LUAD. Additionally, we employed TIMER2.0 to examine the relationship between T-cell infiltration levels and *PPIF* expression across different tumor types within TCGA database. Our analysis revealed that *PPIF* has a stronger correlation with Th2 cells compared to Th1 cells across multiple tumor types (*Figure 3C*). Notably, in head and neck squamous cell carcinoma and kidney renal papillary cell carcinoma, the expression of *PPIF* was inversely correlated with Th1-cell infiltration. We then sought to determine whether *PPIF* expression impacts the prognosis of patients with LUAD as a consequence of immune cell infiltration (*Figure 4A*). In patients with LUAD, those with high expression of *PPIF* and higher

infiltration levels of B cells, $CD4^+$ memory T cells, $CD8^+$ T cells, eosinophils, macrophages, Tregs (regulatory T cells), and Th2 cells have a poorer prognosis. Concurrently, patients exhibiting high *PPIF* expression along with lower infiltration levels of basophils, mesenchymal stem cells, natural killer T-cells, and Tregs also have a poorer prognosis. (*Figure 4B*).

PPIF promoted the proliferation of LUAD cells both in vitro and in vivo

Due to the comparatively low expression of PPIF protein in A549 cells and its high expression in PC9 cells (*Figure 5A*), these two cell types were selected for subsequent functional analyses. *PPIF* knockdown was performed via RNA interference and overexpression was performed using plasmids. The transfection efficiency is shown in *Figure 5B*. To verify the carcinogenic effect of *PPIF*, we examined the cell proliferative capacity using CCK-8, EdU, and clone formation assays (*Figure 5C-5E*). Our results demonstrated that *PPIF* knockdown significantly reduced tumor cell proliferation compared to the control, whereas increased expression of *PPIF* facilitated a more rapid tumor cell expansion. For *in vivo* experiments, we employed a nude mouse model of tumorigenesis established using PC9 cells with stable *PPIF* knockdown. Mice in the sh-*PPIF* group exhibited a significantly slower tumor growth rate compared to the mice in the sh-NC group (*Figure 5F,5G*). Additionally, the weight of the tumor tissues in the sh-NC group was considerably lower (*Figure 5H*). Subsequently, both HE and IHC staining confirmed a marked decrease in *PPIF* expression and the proliferation marker Ki67 within the sh-*PPIF* group (*Figure 5I*). Therefore, our experiments in both the *in vitro* and *in vivo* settings confirmed that *PPIF* could enhance the progression of LUAD.

PPIF facilitated cell-cycle progression and dampened mitophagy through the FOXO3a/PINK1–Parkin axis

To pinpoint the precise mechanisms by which *PPIF* enhances cell proliferation, we carried out flow cytometric analysis and electron microscopic evaluations. Flow cytometric analysis revealed that silencing *PPIF* led to a higher fraction of cells in the G1 phase and a reduced fraction in the S and G2 phases (*Figure 6A*). Conversely, *PPIF* overexpression produced the opposite result (*Figure 6B*). We proceeded to corroborate critical cell-cycle-related protein changes associated with *PPIF* expression through Western blotting analysis. We found that the knockdown of *PPIF* in PC9 cells led to the downregulation of cyclin D1, CDK1, CDK4, and cyclin E1. Meanwhile, the inverse outcome was observed when *PPIF* expression was upregulated in A549 cells (*Figure 6C*). Additionally, we initiated a meticulous investigation of cellular structures, centering our analysis on the mitochondrial components. Electron microscopy results showed that a considerable portion of the mitochondria in the *PPIF*-knockdown cells displayed disorganized cristae, vacuolated regions, or signs of engulfment. Conversely, A549 cells with elevated *PPIF* expression showed a discernible improvement in mitochondrial structure (*Figure 6D*). To corroborate the origins of mitochondrial alterations and substantiate the outcomes of preliminary enrichment analysis, we examined several mitophagy-related genes. Western blotting analysis revealed that *PPIF* silencing increased the expression levels of FOXO3a, PINK1, Parkin, Atg5, and LC3B but reduced P62 levels. Conversely, enhanced expression of *PPIF* led to the inverse effect (*Figure 6E*). These results demonstrated that *PPIF* has a potential role in promoting cell-cycle progression and mediating mitophagy.

Discussion

Although therapies for lung cancer have advanced, it persists as one of the deadliest forms of cancer with a dismal 5-year survival rate (18). The urgent identification of novel biomarkers and exploration of molecular mechanisms are imperative. *PPIF*, commonly known as CypD, plays a pivotal role in regulating cell fate and energy metabolism through a multitude of mechanisms (19-21). CypD has been shown to influence tumor progression through multiple mechanisms and appears to exert a dual influence on the fate of tumor cells (22). The negative effect of CypD on tumor progression is notable, as most antineoplastic agents can promote necrosis in tumor cells by activating the CypD-mPTP pathway (23-26). The interaction between CypD and its molecular partners is being increasingly recognized as a contributing factor in the chemoresistance exhibited by some cancers (27-29). Nevertheless, our research, corroborated by findings from other researchers, suggests that *PPIF* acts as a tumor-promoting molecule, driving tumorigenesis. For instance, the oncogene Ras has been reported to upregulate CypD expression via the Raf-1/MEK/ERK signaling pathway (30). Numerous studies have documented that CypD could maintain aerobic glycolysis (31-33), inhibit tumor cell apoptosis (7,34),

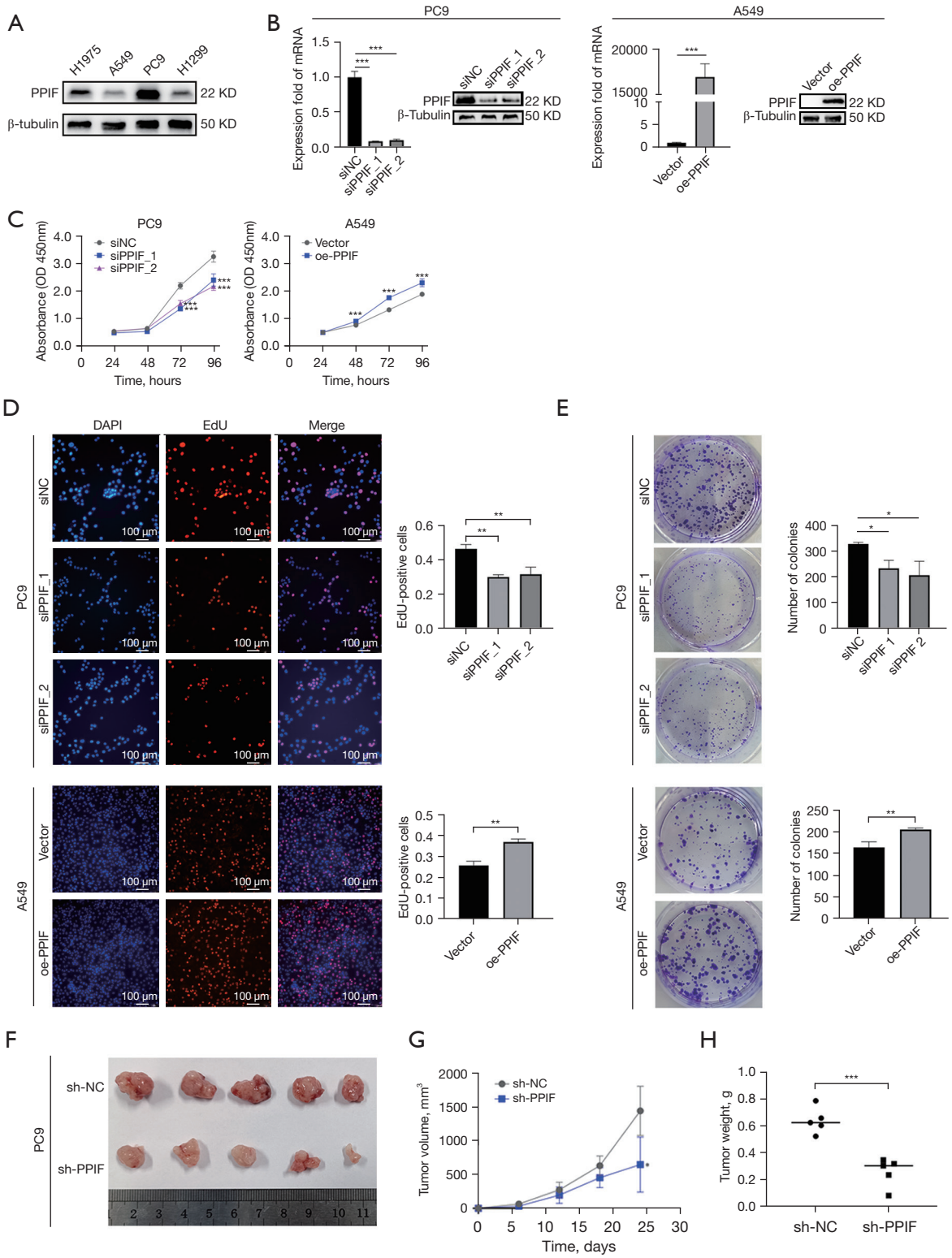

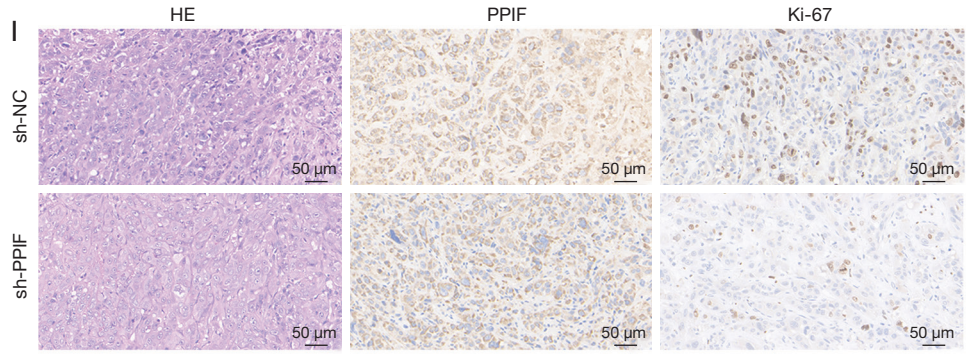

Figure 5 *PPIF* promoted LUAD cell proliferation *in vitro* and *in vivo*. (A) The expression of *PPIF* protein levels in four lung adenocarcinoma cell lines. (B) RT-qPCR and Western blotting assays verified the expression of *PPIF* at 48 h post-transfection. (C-E) CCK-8, EdU, and clone formation assays were executed to confirm the change of the proliferation ability after *PPIF* knockdown in PC9 cells and *PPIF* overexpression in A549 cells. The colonies were stained using crystal violet. (F) Representative images of subcutaneous tumors from different treatment groups. (G) The volume and (H) weight were much lower for xenograft tumors with stable *PPIF* knockdown than for xenograft tumors with negative control. (I) Representative photographs of HE staining and IHC staining of *PPIF* and Ki-67 in different xenograft tumor groups. *, P<0.05; **, P<0.01; ***, P<0.001. RT-qPCR, real-time quantitative polymerase chain reaction; CCK-8, cell counting kit-8; HE, hematoxylin and eosin; IHC, immunohistochemistry; NC, negative control; *PPIF*, peptidyl-prolyl isomerase F; LUAD, lung adenocarcinoma.

and facilitate tumor resistance (35). Our study observed a significant overexpression of *PPIF* in patients with LUAD that correlated with a poor prognosis. Moreover, through cellular and animal model experiments, we established *PPIF* as a promoter of tumor progression in LUAD. However, the precise mechanism underlying *PPIF* upregulation in LUAD remains unconfirmed, necessitating further investigation.

Cyclophilins (Cyps) act as the intracellular receptors for the immunosuppressant drug cyclosporine A (CsA) and perform critical cellular functions mediated by their peptidyl-prolyl cis-trans isomerase (PPIase) activity and chaperone roles (36). We hypothesized that CypD, as a member of the Cyp family, may play a role in modulating immune responses. In psoriasis, elevated *PPIF* expression was found to be associated with the increased immune infiltrates of cells, such as macrophages, activated $CD8^+$ T cells, and aDCs (37). CypD has also been found to be a crucial regulator of T-cell metabolism, pivotal for controlling the expansion of activated T cells (38). Our study found that *PPIF* expression correlated with various immune cell types, such as Tregs, Th2 cells, eosinophils, and B cells. Moreover, *PPIF* expression was found to be correlated with the prognosis in patients with LUAD due to immune cell infiltration. Notably, *PPIF* demonstrated the most significant influence on Th2 cells. Considering the effects of *PPIF* on Th2 and Th1 cells in other tumors, we speculate that *PPIF* may increase the Th2-to-Th1 ratio. Given that tumor immunity is predominantly mediated by cellular immune responses, the immune response elicited by Th1 cells may play a crucial role in suppressing malignant tumor growth. Conversely, an abundance of Th2 cells in patients with tumors may impair cellular immune function, thereby facilitating tumor development and progression. Studies have revealed an overexpression of Th2 cytokines interleukin (IL)-10 and IL-6 in various cancers, including laryngeal and bladder cancer, while Th1 cytokines interferon (IFN)-γ and IL-2 exhibit notably reduced expression levels, indicating a shift from Th1 to Th2 dominance. This immunological shift results in the suppression of the body's cellular immunity (39,40). Therefore, modulating Th1 and Th2 cell differentiation and fostering the proliferation and differentiation of Th0 cells into Th1 cells by inhibiting *PPIF* expression may enhance immune function recovery. This approach could also activate antitumor immune responses and consequently improve the efficacy of comprehensive cancer therapy.

In light of the limited previous research on *PPIF* in oncology, we conducted a functional analysis using GO and KEGG within LUAD. We observed that *PPIF* exhibits a significant correlation with cell mitosis and the progression of the cell cycle. *PPIF* overexpression in LUAD cells accelerates the cell cycle, while its silencing results

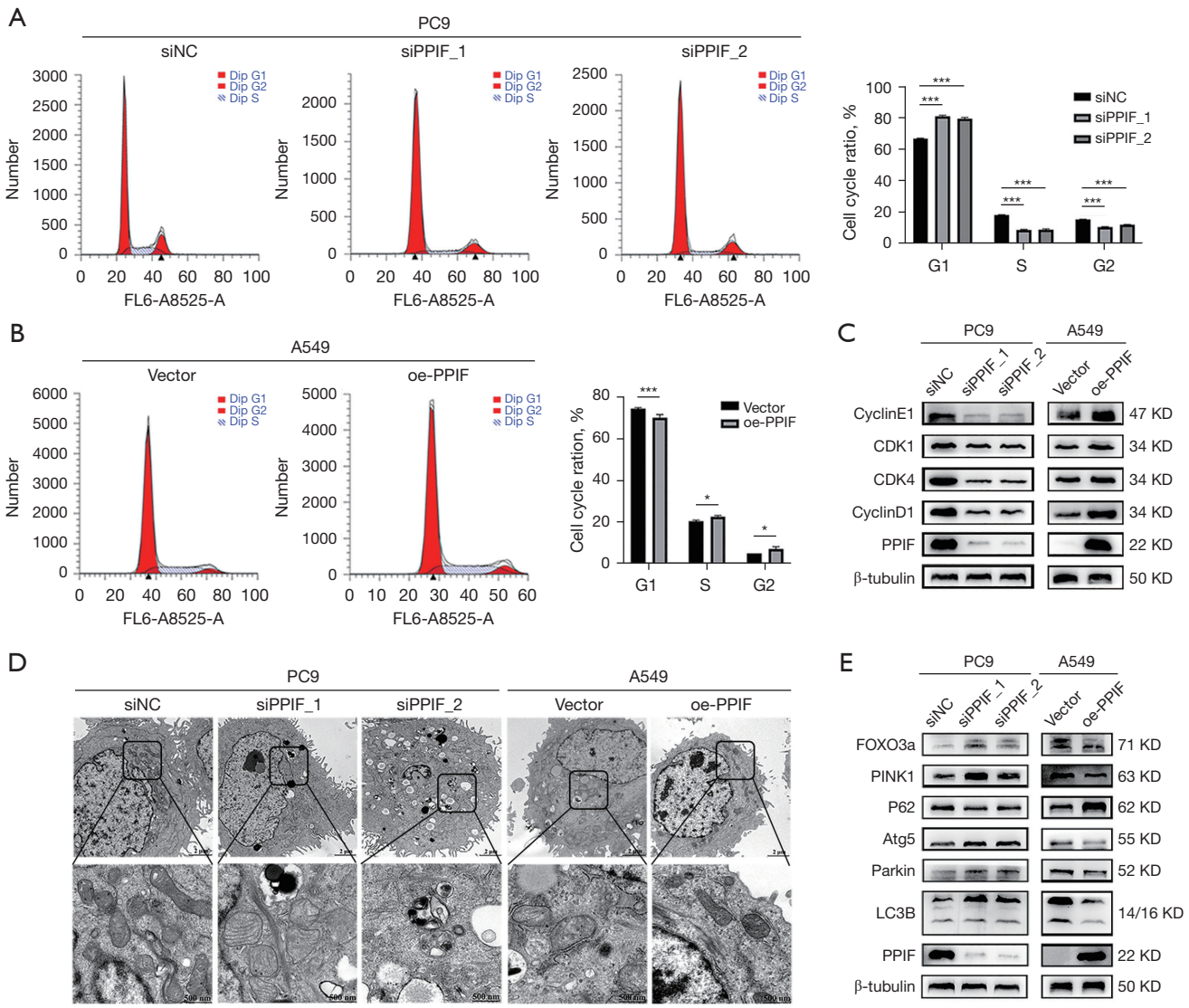

Figure 6 *PPIF* promoted cell-cycle progression and inhibited mitophagy in LUAD cells. Flow cytometry analysis detected the proliferation ability in (A) *PPIF*-knockdown PC9 cells, (B) *PPIF*-overexpression A549 cells, and control cells. (C) The expression of key cell-cycle biomarkers was measured by Western blotting assay. (D) Mitochondrial ultramicrostructure of different groups in A549 and PC9 cells. (E) The expression of FOXO3a/PINK1–Parkin pathway was detected using Western blotting assay. *, P<0.05; ***, P<0.001. *PPIF*, peptidyl-prolyl isomerase F; LUAD, lung adenocarcinoma.

in cell cycle delay. CypD is the sole Cyp localized to the mitochondria. The mechanism by which mitochondrial CypD influences the expression of cell cycle proteins remains elusive. The cyclin D1-CDK4 complex has been shown to relocalize to the mitochondria during the radiation-induced adaptive response, a process that contributes to mitochondrial homeostasis maintenance (41). This establishes the framework for investigating the interactions between CypD, CDK4, and cyclin D1, but the underlying mechanisms warrant further in-depth investigation. While CypD is known to figure prominently in mitochondrial function, the relationship between CypD and mitophagy has not been extensively examined. Our study showed that *PPIF* impedes mitophagy in LUAD cells. Mitophagy in cancer cells may exert dual effects on carcinogenesis and tumor suppression via distinct signaling pathways (42,43). Mitophagy, a selective autophagic process, targets and removes damaged mitochondria,

and thus its role in regulating radiation sensitivity cannot be overlooked (44,45). Ionizing radiation, employed in radiation therapy, results in mitochondrial impairment and functional disruption, which can lead to the buildup of defective organelles. While moderate mitophagy facilitates cellular homeostasis, an excessive autophagic response can precipitate cellular demise. Researchers have found that certain pharmacological agents or the suppression of specific molecules can augment radiosensitivity by enhancing mitophagy (46,47). Our findings indicate the potential of applying *PPIF* inhibition to regulate tumor radiotherapy sensitivity. Interestingly, the KEGG results indicated that *PPIF* affects the FoxO signaling pathway. As a key member of the FoxO family, transcription factor FOXO3a serves as an upstream regulator of mitophagy (48). The PINK1-Parkin signaling cascade constitutes the archetypal pathway for the induction of mitophagy. PINK1 facilitates mitochondrial adaptation to oxidative stress and protects cellular function under the regulation of FOXO3a (49-51). Additionally, we found that *PPIF* suppresses FOXO3a/PINK1-Parkin-mediated mitophagy. However, the precise molecular mechanisms underlying *PPIF* modulation of FOXO3a/PINK1-Parkin signaling require further investigation. Moreover, FOXO3a functions as a tumor-suppressor gene and plays a significant role in the development of resistance to chemotherapy (52-55). The identification of *PPIF*-mediated inhibition of FOXO3a would help to explain the *PPIF*-promoted development of LUAD that was observed in our study.

It is noteworthy that, research by Zhang *et al.* suggests a potential link between CypD and the development of chronic obstructive pulmonary disease (COPD) (56), which is also a common comorbidity in lung cancer patients (57). Patients with COPD have a higher risk of developing lung cancer, which is due to the fact that long-term chronic inflammation and lung damage may lead to abnormal cell proliferation and carcinogenesis. Concurrently, the incidence of COPD in patients with lung cancer is also elevated. The pathogenesis of lung cancer and COPD has similarities, and smoking may also be common etiologies for both diseases. CypD could be involved in COPD pathogenesis through its effects on mitochondrial function and cell death pathways, the involvement of CypD in mitochondrial dysfunction could exacerbate oxidative stress—key factors in COPD and lung cancer (57-60). If CypD is indeed a critical element in the development of both COPD and lung cancer, this could provide a significant insight into the molecular mechanisms driving these diseases. The common features of COPD and lung cancer, such as inflammation, cell proliferation, and oxidative stress, might be modulated by the activity of CypD. Studies focused on CypD's function within these pathways could facilitate the identification of novel biomarkers for early detection and provide potential targets for therapeutic interventions.

The potential clinical applications of the *PPIF* gene in LUAD treatment are substantial. Due to its overexpression in LUAD and independent prognostic value, *PPIF* could serve as a biomarker for disease severity and patient outcomes. Targeting *PPIF* may inhibit LUAD cell proliferation and alter cell cycle dynamics. Additionally, *PPIF*'s involvement in immune modulation suggests that therapies affecting this gene could possibly enhance immune system targeting of LUAD cells. In future research, we plan to employ liquid biopsies to measure *PPIF* mRNA expression, and further explore its potential as a predictive indicator for the efficacy of immunotherapy. The ability of *PPIF* to hinder mitophagy by affecting the FOXO3a/PINK1-Parkin pathway also presents an opportunity to disrupt cancer cell metabolism.

Limitations

This study encompassed several limitations. Firstly, the analyses in this study were conducted using data from multiple public databases. It is acknowledged that web-based databases such as UCSC Xena, GEPIA2, TIMER2.0, Kaplan-Meier plotter, and BioGRID may not provide comprehensive details regarding data provenance and methodological approaches, representing a notable limitation of this research. Secondly, further *in vivo* and *in vitro* research is essential to elucidate the molecular mechanisms by which *PPIF* regulates immune cell infiltration in LUAD. Thirdly, future prospective studies involving larger cohorts are warranted to assess the prognostic significance of *PPIF*.

Conclusions

Our research reveals that *PPIF* promotes LUAD progression by regulating immune cell infiltration, cell-cycle dynamics, and mitophagy. Consequently, inhibiting *PPIF* could represent a novel therapeutic strategy for patients with LUAD, and further research involving larger sample sizes and more comprehensive experiments are warranted to explore its potential.

Acknowledgments

We wish to express our gratitude to the individuals and organizations who contributed to the public databases used in this study.

Funding: This study was supported by the National Key Research and Development Program (Nos. 2021YFC2500900, 2021YFC2500904, and 2021YFC2500905), the Natural Science Foundation of Shandong Province (No. ZR2021LSW006), and the Taishan Scholar Program of Shandong Province (No. ts201712087).

Footnote

Reporting Checklist: The authors have completed the MDAR and ARRIVE reporting checklists. Available at https://tlcr.amegroups.com/article/view/10.21037/tlcr-24-344/rc

Data Sharing Statement: Available at https://tlcr.amegroups.com/article/view/10.21037/tlcr-24-344/dss

Peer Review File: Available at https://tlcr.amegroups.com/article/view/10.21037/tlcr-24-344/prf

Conflicts of Interest: All authors have completed the ICMJE uniform disclosure form (available at https://tlcr.amegroups.com/article/view/10.21037/tlcr-24-344/coif). L.K. received honoraria from German Cancer Society, AstraZeneca and Art Tempi. L.K. received support for attending meetings and travel from AstraZeneca, European Society for Medical Oncology (ESMO) and German Cancer Society (DKG). L.K. receives an unrestricted grant (NCT05027165) to his clinic. In addition, L.K. receives grants from AMGEN and Art Tempi to him. W.M.B. received consulting fees, payments or honoraria, payments for expert testimony and payments of participation in advisory boards from the following companies: AstraZeneca, BMS, Daiichi-Sankyo, MSD, Lilly, Pfizer, Sanofi, Roche, Takeda and received travel support to congresses from AstraZeneca, Lilly and Daiichi-Sankyo. The other authors have no conflicts of interest to declare.

Ethical Statement: The authors are accountable for all aspects of the work in ensuring that questions related to the accuracy or integrity of any part of the work are appropriately investigated and resolved. The experiments involving patients were reviewed and approved by the Medical Ethics Committee of Qilu Hospital of Shandong University (No. KYLL-202008-023-1) and were conducted in accordance with the principles outlined in the Declaration of Helsinki (revised in 2013). Each patient or their legal guardians provided signed informed consent forms. The animal experiments were conducted in accordance with institutional guidelines for the care and use of animals, as authorized by a project license (DWLL-2023-056) issued by the Ethics Committee of Animal Experiment of Qilu Hospital of Shandong University.

References

1. Riano I, Dragnev KH, Phillips JD. The beginning of the perioperative immunotherapy era in early-stage non-small cell lung cancer. Transl Lung Cancer Res 2023;12:2359-65.
2. Choi DH, Jung HA, Park S, et al. Effectiveness and safety of amivantamab in EGFR exon 20 insertion (E20I) mutations in non-small cell lung cancer (NSCLC). Transl Lung Cancer Res 2023;12:2448-59.
3. Sentana-Lledo D, Academia E, Viray H, et al. EGFR exon 20 insertion mutations and ERBB2 mutations in lung cancer: a narrative review on approved targeted therapies from oral kinase inhibitors to antibody-drug conjugates. Transl Lung Cancer Res 2023;12:1590-610.
4. Baines CP, Kaiser RA, Purcell NH, et al. Loss of cyclophilin D reveals a critical role for mitochondrial permeability transition in cell death. Nature 2005;434:658-62.
5. Nakagawa T, Shimizu S, Watanabe T, et al. Cyclophilin D-dependent mitochondrial permeability transition regulates some necrotic but not apoptotic cell death. Nature 2005;434:652-8.
6. Eliseev RA, Malecki J, Lester T, et al. Cyclophilin D interacts with Bcl2 and exerts an anti-apoptotic effect. J Biol Chem 2009;284:9692-9.
7. Schubert A, Grimm S. Cyclophilin D, a component of the permeability transition-pore, is an apoptosis repressor.

Cancer Res 2004;64:85-93.
8. Yang L, Cui Y, Sun X, et al. Overexpression of TICRR and PPIF confer poor prognosis in endometrial cancer identified by gene co-expression network analysis. Aging (Albany NY) 2021;13:4564-89.
9. Jia J, Xia J, Liu W, et al. Cinnamtannin B-1 Inhibits the Progression of Osteosarcoma by Regulating the miR-1281/PPIF Axis. Biol Pharm Bull 2023;46:67-73.
10. Blum A, Wang P, Zenklusen JC. SnapShot: TCGA-Analyzed Tumors. Cell 2018;173:530.
11. Stark C, Breitkreutz BJ, Reguly T, et al. BioGRID: a general repository for interaction datasets. Nucleic Acids Res 2006;34:D535-9.
12. Nagy Á, Munkácsy G, Győrffy B. Pancancer survival analysis of cancer hallmark genes. Sci Rep 2021;11:6047.
13. Ashburner M, Ball CA, Blake JA, et al. Gene ontology: tool for the unification of biology. The Gene Ontology Consortium. Nat Genet 2000;25:25-9.
14. Kanehisa M, Goto S, Sato Y, et al. KEGG for integration and interpretation of large-scale molecular data sets. Nucleic Acids Res 2012;40:D109-14.
15. Subramanian A, Tamayo P, Mootha VK, et al. Gene set enrichment analysis: a knowledge-based approach for interpreting genome-wide expression profiles. Proc Natl Acad Sci U S A 2005;102:15545-50.
16. Hänzelmann S, Castelo R, Guinney J. GSVA: gene set variation analysis for microarray and RNA-seq data. BMC Bioinformatics 2013;14:7.
17. Bindea G, Mlecnik B, Tosolini M, et al. Spatiotemporal dynamics of intratumoral immune cells reveal the immune landscape in human cancer. Immunity 2013;39:782-95.
18. Meador CB, Hata AN. Acquired resistance to targeted therapies in NSCLC: Updates and evolving insights. Pharmacol Ther 2020;210:107522.
19. Beutner G, Alanzalon RE, Porter GA Jr. Cyclophilin D regulates the dynamic assembly of mitochondrial ATP synthase into synthasomes. Sci Rep 2017;7:14488.
20. Gauba E, Chen H, Guo L, et al. Cyclophilin D deficiency attenuates mitochondrial F1Fo ATP synthase dysfunction via OSCP in Alzheimer's disease. Neurobiol Dis 2019;121:138-47.
21. Gauba E, Guo L, Du H. Cyclophilin D Promotes Brain Mitochondrial F1FO ATP Synthase Dysfunction in Aging Mice. J Alzheimers Dis 2017;55:1351-62.
22. Zhang L, Liu Y, Zhou R, et al. Cyclophilin D: Guardian or Executioner for Tumor Cells? Front Oncol 2022;12:939588.
23. Ying L, Chunxia Y, Wei L. Inhibition of ovarian cancer cell growth by a novel TAK1 inhibitor LYTAK1. Cancer Chemother Pharmacol 2015;76:641-50.
24. Minjie S, Defei H, Zhimin H, et al. Targeting pancreatic cancer cells by a novel hydroxamate-based histone deacetylase (HDAC) inhibitor ST-3595. Tumour Biol 2015;36:9015-22.
25. Pan H, Wang BH, Lv W, et al. Esculetin induces apoptosis in human gastric cancer cells through a cyclophilin D-mediated mitochondrial permeability transition pore associated with ROS. Chem Biol Interact 2015;242:51-60.
26. Kai S, Lu JH, Hui PP, et al. Pre-clinical evaluation of cinobufotalin as a potential anti-lung cancer agent. Biochem Biophys Res Commun 2014;452:768-74.
27. Wu PK, Hong SK, Park JI. Mortalin depletion induces MEK/ERK-dependent and ANT/CypD-mediated death in vemurafenib-resistant B-Raf(V600E) melanoma cells. Cancer Lett 2021;502:25-33.
28. Wu PK, Hong SK, Chen W, et al. Mortalin (HSPA9) facilitates BRAF-mutant tumor cell survival by suppressing ANT3-mediated mitochondrial membrane permeability. Sci Signal 2020;13:eaay1478.
29. Chen SH, Li DL, Yang F, et al. Gemcitabine-induced pancreatic cancer cell death is associated with MST1/cyclophilin D mitochondrial complexation. Biochimie 2014;103:71-9.
30. Bigi A, Beltrami E, Trinei M, et al. Cyclophilin D counteracts P53-mediated growth arrest and promotes Ras tumorigenesis. Oncogene 2016;35:5132-43.
31. Nederlof R, van den Elshout MAM, Koeman A, et al. Cyclophilin D ablation is associated with increased end-ischemic mitochondrial hexokinase activity. Sci Rep 2017;7:12749.
32. Giang AH, Raymond T, Brookes P, et al. Mitochondrial dysfunction and permeability transition in osteosarcoma cells showing the Warburg effect. J Biol Chem 2013;288:33303-11.
33. Liu Z, Li L, Xue B. Effect of ganoderic acid D on colon cancer Warburg effect: Role of SIRT3/cyclophilin D. Eur J Pharmacol 2018;824:72-7.
34. Talari NK, Panigrahi MK, Madigubba S, et al. Overexpression of aryl hydrocarbon receptor (AHR) signalling pathway in human meningioma. J Neurooncol 2018;137:241-8.
35. Ghosh JC, Siegelin MD, Vaira V, et al. Adaptive mitochondrial reprogramming and resistance to PI3K therapy. J Natl Cancer Inst 2015;107:dju502.
36. Lee J, Kim SS. Current implications of cyclophilins in human cancers. J Exp Clin Cancer Res 2010;29:97.

37. Li Y, Li L, Tian Y, et al. Identification of novel immune subtypes and potential hub genes of patients with psoriasis. J Transl Med 2023;21:182.
38. Tzelepis F, Blagih J, Khan N, et al. Mitochondrial cyclophilin D regulates T cell metabolic responses and disease tolerance to tuberculosis. Sci Immunol 2018;3:eaar4135.
39. Xu X, Wang R, Su Q, et al. Expression of Th1- Th2- and Th17-associated cytokines in laryngeal carcinoma. Oncol Lett 2016;12:1941-8.
40. Satyam A, Singh P, Badjatia N, et al. A disproportion of TH1/TH2 cytokines with predominance of TH2, in urothelial carcinoma of bladder. Urol Oncol 2011;29:58-65.
41. Jin C, Qin L, Shi Y, et al. CDK4-mediated MnSOD activation and mitochondrial homeostasis in radioadaptive protection. Free Radic Biol Med 2015;81:77-87.
42. Mizushima N, Levine B. Autophagy in Human Diseases. N Engl J Med 2020;383:1564-76.
43. Li L, Hu F. Mitophagy in tumor: foe or friend?. Endokrynol Pol 2023;74:511-9.
44. Zhang Y, Pang C, Zhang C, et al. HILPDA-mediated lipidomic remodelling promotes radiotherapy resistance in nasopharyngeal carcinoma by accelerating mitophagy. Cell Mol Life Sci 2023;80:242.
45. Wei Y, Xiao G, Xu H, et al. Radiation resistance of cancer cells caused by mitochondrial dysfunction depends on SIRT3-mediated mitophagy. FEBS J 2023;290:3629-45.
46. Chang M, Song X, Geng X, et al. Temozolomide-Perillyl alcohol conjugate impairs Mitophagy flux by inducing lysosomal dysfunction in non-small cell lung Cancer cells and sensitizes them to irradiation. J Exp Clin Cancer Res 2018;37:250.
47. Wang R, Shang Y, Chen B, et al. Protein disulfide isomerase blocks the interaction of LC3II-PHB2 and promotes mTOR signaling to regulate autophagy and radio/chemo-sensitivity. Cell Death Dis 2022;13:851.
48. Yu W, Gao B, Li N, et al. Sirt3 deficiency exacerbates diabetic cardiac dysfunction: Role of Foxo3A-Parkin-mediated mitophagy. Biochim Biophys Acta Mol Basis Dis 2017;1863:1973-83.
49. Hoshino A, Ariyoshi M, Okawa Y, et al. Inhibition of p53 preserves Parkin-mediated mitophagy and pancreatic β-cell function in diabetes. Proc Natl Acad Sci U S A 2014;111:3116-21.
50. Hoshino A, Mita Y, Okawa Y, et al. Cytosolic p53 inhibits Parkin-mediated mitophagy and promotes mitochondrial dysfunction in the mouse heart. Nat Commun 2013;4:2308.
51. Rask-Madsen C, King GL. Vascular complications of diabetes: mechanisms of injury and protective factors. Cell Metab 2013;17:20-33.
52. Li H, Yuan Y, Dong H, et al. Foxo3a-Mediated DNMT3B Impedes Cervical Cancer Cell Proliferation and Migration Capacities through Suppressing PTEN Promoter Methylation. J Invest Surg 2023;36:2162170.
53. Prabhu VV, Allen JE, Dicker DT, et al. Small-Molecule ONC201/TIC10 Targets Chemotherapy-Resistant Colorectal Cancer Stem-like Cells in an Akt/Foxo3a/TRAIL-Dependent Manner. Cancer Res 2015;75:1423-32.
54. Tang Z, Zhang Y, Yu Z, et al. Metformin Suppresses Stemness of Non-Small-Cell Lung Cancer Induced by Paclitaxel through FOXO3a. Int J Mol Sci 2023;24:16611.
55. Lu D, Liu R, Zhou Y, et al. FOXO3a-dependent up-regulation of HSP90 alleviates cisplatin-induced apoptosis by activating FUNDC1-mediated mitophagy in hypoxic osteosarcoma cells. Cell Signal 2023;101:110500.
56. Zhang R, Shan H, Li Y, et al. Cyclophilin D Contributes to Airway Epithelial Mitochondrial Damage in Chronic Obstructive Pulmonary Disease. Lung 2023;201:287-95.
57. Park HY, Kang D, Lee H, et al. Impact of chronic obstructive pulmonary disease on mortality: A large national cohort study. Respirology 2020;25:726-34.
58. Barnes PJ. Oxidative stress-based therapeutics in COPD. Redox Biol 2020;33:101544.
59. Taniguchi A, Tsuge M, Miyahara N, et al. Reactive Oxygen Species and Antioxidative Defense in Chronic Obstructive Pulmonary Disease. Antioxidants (Basel) 2021;10:1537.
60. Finicelli M, Digilio FA, Galderisi U, et al. The Emerging Role of Macrophages in Chronic Obstructive Pulmonary Disease: The Potential Impact of Oxidative Stress and Extracellular Vesicle on Macrophage Polarization and Function. Antioxidants (Basel) 2022;11:464.

Cite this article as: Feng Z, Yuan L, Ma L, Yu W, Kheir F, Käsmann L, Brueckl WM, Jin K, Wang D, Shen Y, Li R, Tian H. Peptidyl-prolyl isomerase F as a prognostic biomarker associated with immune infiltrates and mitophagy in lung adenocarcinoma. Transl Lung Cancer Res 2024;13(6):1346-1364. doi: 10.21037/tlcr-24-344